Ethylene Removal by Adsorption and Photocatalytic Oxidation using Biocarbon –TiO_2 Nanocomposites

Ana M. Regadera-Macías, Sergio Morales-Torres, Luisa M. Pastrana-Martínez*, Francisco J. Maldonado-Hódar

NanoTech – Nanomaterials and Sustainable Chemicals Technologies, Department of Inorganic Chemistry, Faculty of Science, University of Granada, Avda. Fuente Nueva, s/n, ES18071 Granada, Spain

**Corresponding author: lpastrana@ugr.es (Luisa M Pastrana-Martínez), Tel. +34 958248489.*

Abstract

A series of adsorbents and photocatalysts were developed using agricultural residues (olive stones) as raw materials. Activated carbons (ACs) were synthesized by physical activation and posteriorly, impregnated with TiO_2 by a hydrothermal method. Both adsorbents (ACs) and composites (carbon-TiO_2) were texturally, morphologically and chemically characterized by using complementary techniques (i.e. SEM, gas adsorption, TG, XRD, pH_{PZC}, and so on) and then, the affinity of these samples for the ethylene molecules was tested in columns under dynamic conditions. The corresponding breakthrough curves were determined obtaining the amounts adsorbed at the breakthrough and saturation points. Finally, the photooxidation of ethylene to CO_2 using carbon-TiO_2 composites was analysed under UV-Vis and near UV-Vis irradiations. The physicochemical characteristics of supports and composites were correlated with their ability to remove ethylene, looking to identify the parameters allowing to improve the performance of the samples.

Keywords*: Adsorption; heterogeneous photocatalysis; TiO_2; nanorods; activated carbon; ethylene.*

1. Introduction

Perishable food products are spoiled from the moment they are harvested. Therefore, their classification and packaging is processed as quickly as possible, and then, they are stored and transported in cold chambers, where different types of atmospheres (i.e. normal, modified, controlled and dynamic) are used to regulate both O_2 and CO_2 levels and retard maturation. Moreover, stored fruits and vegetables release different gases like ethylene (C_2H_4), which in turn, acts as a hormone, accelerating the ripening process. Consequently, the ethylene removal from this environment is a critical step because, even at a very low concentration, it may induce ripening and senescence, increasing the proportion of rejection with the consequent economic loss [1, 2]. Ethylene can be removed by adsorption, recirculating the air in the chambers through the appropriate filters [3], oxidised to CO_2 using chemicals such as $KMnO_4$ [4], or thermal oxidation at elevated temperatures (200-300 ºC) [5]. Heterogeneous photocatalytic combustion is an interesting process to remove ethylene at room temperature and under solar radiation, but this requires the development of suitable photocatalysts [6]. So far, the most studied semiconductor for the elimination of pollutants is titanium dioxide (TiO_2), which have been proved to be a promising material in different photocatalytic systems because of its low toxicity, cost effectiveness, high efficiency under UV irradiation and stability [7, 8]. However, its application in the visible range of the solar spectrum is limited by the low quantum yield and the wide band gap of TiO_2, so the electrons from TiO_2 valence band can only be activated under UV radiation [7, 9]. Several strategies have been developed to expand the response of TiO_2 into the visible range, namely the addition of electron donors [10], metal cation or anion doping [11], dye sensitization [12], formation of exposed (001) facets [13], coupling of TiO_2 nanostructures on supports such as, carbon materials [14-16] among others.

Carbon materials have demonstrated their ability to enhance the photocatalytic performance of TiO_2 by producing a synergistic effect between phases [17], not only based on a stronger adsorptive activity, but also because the conjugated π-bond system in carbons could accept the photogenerated electrons (i.e., sensitizer), and avoiding the electron-hole recombination. In previous research, TiO_2 was used for degradation of ethylene increasing the photocatalytic performance by optimizing the nanoparticle characteristics [18, 19]. The carbon support properties could also influence on the interactions between

phases and corresponding performance of supported nanocomposites. Thus, composites using nitrogen-doped reduced graphene (N-GR/TiO_2) as support showed a lower efficiency than undoped graphene (GR/TiO_2) for the ethylene photodegradation [20]. The formation of reactive oxygen species (ROS) in the photocatalytic process, which in turn provoke the oxidation of the C_2H_4 molecules is well known involving equations (1-7) [21, 22]. The $^{\bullet}OH$ and $^{\bullet}O_2^-$ radicals, which could be produced, may react with ethylene to produce carbon dioxide and water through the overall equation 8.

$$TiO_2 + h\nu \rightarrow TiO_2 + h^+ + e^- \quad (1)$$

$$h^+ + H_2O \rightarrow {}^{\bullet}OH + H^+ \quad (2)$$

$$e^- + O_2 \rightarrow {}^{\bullet}O_2^- \quad (3)$$

$$^{\bullet}O_2^- + H^+ \rightarrow {}^{\bullet}HO_2 \quad (4)$$

$$2\ {}^{\bullet}HO_2 \rightarrow O_2 + H_2O_2 \quad (5)$$

$$H_2O_2 + {}^{\bullet}O_2^- \rightarrow {}^{\bullet}OH + OH^- + O_2 \quad (6)$$

$$h^+ + OH^- \rightarrow {}^{\bullet}OH \quad (7)$$

$$C_2H_4 + 3O_2 \rightarrow 2CO_2 + 2H_2O \quad (8)$$

In this manuscript, both processes, adsorption and photooxidation, are attempted for the ethylene removal by means of composites with high porosity and surface area, provided by biocarbons used as supports of nanostructured active phases (TiO_2 nanorods), looking for the synergism between both phases. Simultaneously, the use of agricultural waste for the production of cheap materials to be applied in the agro-food industry, according to the principles of the circular economy, could economically favour the implementation of the developed technology. To our knowledge this is the first comprehensive study using bioresidues as raw materials with suitable adsorption and photocatalytic performance towards the selective ethylene removal to CO_2 under continuous flow and humidity conditions. Synthesis conditions, the obtained physicochemical properties and the achieved performance for the materials will be analyzed and correlated in order to identify the key parameters that should be enhanced to obtain active and cheap 2-in-1 adsorbents/photocatalysts, suitable for the ethylene removal from storage chambers of perishable fruits.

2. Materials and methods

2.1. Sample preparation

Olive stones (OS) were selected as raw materials for the preparation of ACs used as adsorbents or photocatalyst supports. Samples were prepared by a two-step process including a carbonization of OS carried out at 850 ºC for 2 h in N_2 flow, followed by physical activation with steam at 800 ºC for 4 or 6 h, leading to AC13 and AC23 samples. A commercial AC (Norit® RX-3 Extra) and Evonik Aeroxide® TiO_2 P25 (80% anatase/20% rutile) was used as a reference and raw materials. Carbon-TiO_2 composites were prepared in a mass ratio of 1:1 weight base, by hydrothermal deposition at 150 ºC for 48 h. Finally, the obtained powders were pre-treated at 300 ºC in air atmosphere to enhance the crystallinity of the TiO_2 nanorods [23]. Reference TiO_2 nanorods (TiO_2 NRs) were also prepared following the same procedure, but without adding AC. Additional details are summarized in the supplementary material section.

2.2. Sample characterization

Pure carbon, TiO_2 and their corresponding composites were deeply characterized by complementary techniques such as thermogravimetric (TG) analysis, physical adsorption of N_2 and CO_2, point of zero charge (pH_{PZC}), scanning electron microscopy (SEM), X-ray diffraction (XRD) and UV-Vis diffuse reflectance, according to the procedures detailed in the supplementary material section.

2.3. Adsorption and photocatalytic performance

Adsorption and photocatalytic experiments were carried out in glass or quartz reactors, operating in continuous mode at atmospheric pressure and using a fixed bed of 10 × 0.6 cm, i.e. 0.3-0.5 g of material (Figure S1). The adsorption capacity of the samples was determined in dry conditions using a calibrated C_2H_4 / N_2 cylinder (1000 vppm). The breakthrough curves were obtained by analysing the amount of C_2H_4 at the column outlet by gas chromatography (GC) using a Shimadzu GC-2010 Plus equipped with a BID detector and a Rt-Q-BOND Column as a function of time. From the analysis of these curves, it

may be determined the breakthrough and saturation points, i.e. the C_2H_4 concentration at the column outlet reaching 2 and 90% of the initial concentration.

Photocatalytic experiments were carried out using a mixture of C_2H_4/Air/H_2O with a C_2H_4 concentration of 50 vppm and 50% of relative humidity (RH). The reactor was irradiated using a medium-pressure mercury lamp (125 W, mod. 3010/PX0686) from Photochemical Reactors LTD., equipped with a glass water cooling jacket to obtain irradiation in the near UV-Vis range ($\lambda > 350$ nm, corresponding to the 74% of the lamp emission). Experiments carried out in a quartz reactor and with a quartz water cooling jacket were also performed to analyze the effect of the whole UV-Vis range from the lamp (λ_{main} = 254, 313, 366, 436 and 546 nm) on the photocatalytic performance. The amounts of transformed C_2H_4 and formed CO_2, as unique reaction product observed, were also monitored by GC during the reaction time. Additional details are summarized in the supplementary material section.

3. Results and discussion

3.1. Sample characterization

The composition and stability of the carbon/TiO_2 composites was analyzed by burning off the organic phase, these experiments being also followed by thermogravimetric analysis. The TG curves for the carbon-TiO_2 composites showed a proportion of the different phases in good agreement with those theoretical TiO_2 loadings, i.e. ≈ 50 wt.% (Figure S2a). Moreover, all composites are stable in air up to around 550 ºC, where an important weight loss occurs as consequence of the carbon combustion. The small weight loss observed below 200 ºC should be associated to water desorption.

The morphology of the different materials was analyzed by SEM (Figure 1). All biocarbons presented a very open and porous structure with large cavities remaining from the lignocellulosic character of the raw materials, as observed in Figure 1a for the AC13 sample as an example. As expected, pure TiO_2 obtained by the hydrothermal method was formed by nanorods of different diameters (Figure 1b). In the case of the composites, both structures are clearly identified when biocarbon supports were used (e.g. AC13-TiO_2 in Figure 1c and inset), whereas when commercial Norit AC was used as support (i.e. Norit-

TiO_2), TiO_2 was not nanostructured as nanorods and in general, spherical particles were observed (Figure 1d). Of note, the narrower diameter of TiO_2 nanorods and the intimate contact between phases observed for AC13-TiO_2 (Figure 1c).

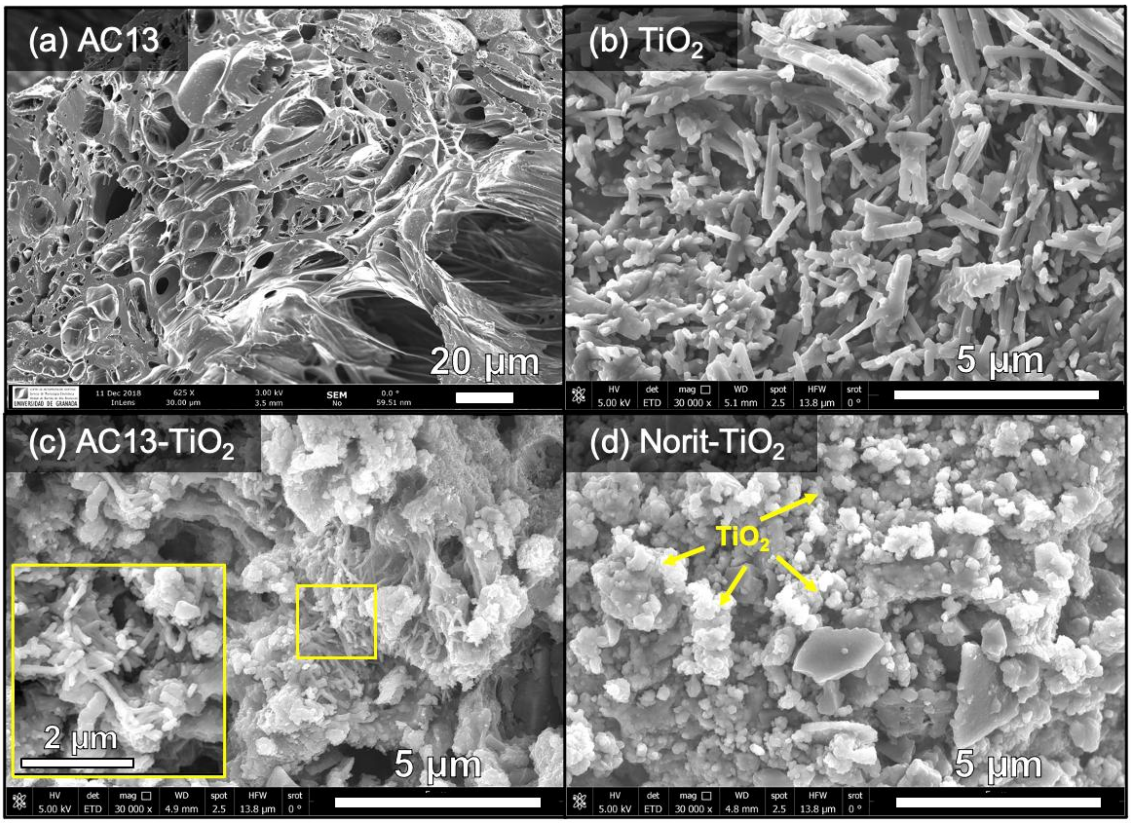

Figure 1. SEM micrographs of (a) AC13, (b) TiO_2 NRs, (c) AC13-TiO_2 (a higher magnification in the inset) and (d) Norit-TiO_2.

Textural characteristics of the materials were analyzed by physical adsorption of N_2 and CO_2 at – 196 ºC and 0 ºC, respectively, which results are compiled in Table 1 and Figure S3. It is noteworthy the strong similarity between the porosity of commercial Norit AC and those obtained by physical activation of olive stones (i.e. AC13 and AC23). In general, all carbon supports presented adsorption isotherms of type I, in accordance with IUPAC classification, typical of microporous materials [24]. The N_2 adsorption-desorption isotherms are very close between them (black lines in Figure S3), although the neck of the adsorption branch of the isotherm is larger in the case of Norit than for the other biocarbons, denoting a more heterogeneous microporosity. Thus, they showed similar values of the BET surface area (S_{BET}) of around 1200-1330 $m^2\ g^{-1}$ and a total pore volume (V_T) between 0.55-0.58 $cm^3\ g^{-1}$ (Table

1). The main differences are observed in the microporosity range. The DR equation confirms that the microporosity accessible to N_2 is wider in the Norit sample than for both biocarbons, increasing the microporous surface (S_{mic}) from 603 to 916 m^2 g^{-1} for Norit and AC23, respectively. This narrower microporosity leads to higher micropore surfaces determined from the CO_2 adsorption isotherms, associated to narrow micropores (diameter < 0.7 nm). On the contrary, the mesopore volume (V_{meso}) and hysteresis cycle in the isotherms from $p/p_0 > 0.4$ was larger for Norit than for ACs prepared from olive stones (Table 1). On the other hand, the TiO_2 NRs showed a isotherm of type II, in accordance with IUPAC classification, characteristic of macroporous materials or materials presenting a low porosity [24] (Figure S3a). Compared to the carbon supports, the titania nanorods are mainly mesoporous with a smaller S_{BET}. Nevertheless, this parameter increased three-times regarding the raw Aeroxide P25 (from 57 to 185 m^2 g^{-1}), showing the strong influence of the nanostructure fitting after recrystallization during the hydrothermal treatment.

Concerning the porosity of the carbon-TiO_2 composites (blue lines in Figure S3), textural characteristics showed the combination of microporous carbon supports and the mesoporous active TiO_2 phases. In general, W_0 decreased but the mean micropore size (L_0) increased, denoting the blockage of the microporosity by the deposition of TiO_2 and leading to a lower S_{BET} and S_{mic} with the addition of TiO_2 (Table 1). On the contrary, the enhancement of the mesoporosity observed for the composites in comparison with the biocarbon supports is due to the formation of TiO_2 nanorods, as showed by SEM images (Figure 1). However, using the commercial Norit, TiO_2 shows spherical nanoparticles (Norit-TiO_2, Figure 1d), which do not modify the original mesoporosity of the support. In spite of the similarities described on the N_2 adsorption isotherms, SEM images showed a very open structure of biochars, with a significant number of large macroporous channels in the range of micrometres, which can allow the recrystallization of TiO_2 phases inside the biocarbon cavities.

Table 1. Textural characteristics and point of zero charge (pH_{PZC}) of biocarbons and their corresponding carbon-TiO_2 composites.

Sample	N_2 adsorption						CO_2 adsorption			pH_{PZC}
	S_{BET} (m^2 g^{-1})	W_0 (cm^3 g^{-1})	L_0 (nm)	S_{mic} (m^2 g^{-1})	V_{meso} (cm^3 g^{-1})	V_T (cm^3 g^{-1})	W_0 (cm^3 g^{-1})	L_0 (nm)	S_{mic} (m^2 g^{-1})	

Norit	1203	0.51	1.68	603	0.10	0.57	0.30	0.71	831	10.2
AC13	1328	0.55	1.23	887	0.04	0.58	0.43	0.75	1157	8.8
AC23	1253	0.51	1.14	916	0.04	0.55	0.47	0.75	1267	6.7
TiO_2 NRs	185	0.07	1.46	95	0.47	0.60	-	-	-	4.7
Norit-TiO_2	600	0.25	1.20	407	0.07	0.33	0.23	0.75	617	8.7
AC13-TiO_2	752	0.31	1.31	466	0.39	0.74	0.23	0.70	656	8.3
AC23-TiO_2	680	0.27	1.48	367	0.34	0.66	0.18	0.72	502	6.4

S_{BET}= BET surface area; W_0= micropore volume; L_0= mean micropore width; S_{mic}= microporous surface; V_{meso}= mesoporous volume; V_T= total pore volume.

The chemical characterization of supports and composites was carried out by the determination of their pH_{PZC} (Table 1). Although all carbon materials had a basic character, it is noteworthy the highest pH_{PZC} value of Norit regarding the biocarbons. In addition, this parameter decreases with increasing the activation degree (i.e. 8.8 and 6.7 for AC13 and AC23, respectively), which could be related with a progressive oxidation of the carbon surface during prolongated activation times. On contrast, TiO_2 possessed a weak acidic character, mainly related with the presence of Lewis-acid sites [25]. Thus, although the pH_{PZC} decreased for all the composites compared to their corresponding carbon supports, their acidity increased as follows: Norit-TiO_2 < AC13-TiO_2 < AC23-TiO_2.

The crystallinity of the samples was analysed by XRD (Figure 2). Pure TiO_2 nanorods present the typical anatase pattern (JCPDS No. 21-1272) with the characteristic diffraction peaks at 25.2, 37.7, 48.1, 53.5 and 63.1º [26]. Nonetheless, significant differences were observed for the diffractograms of composites, suggesting a mixture of crystalline phases. Hence, the (101) diffraction of the anatase placed at 25.3º was not the main peak in most of the cases, because the peak at 48.1º due to the (200) diffraction of anatase was overlapping with the (231) diffraction of brookite phase (JCPDS No. 16-617). The presence of brookite takes place particularly in the composites prepared using biocarbon supports, where different new peaks/bands are observed. For instance, the peak at 25.5º due to the (111) diffraction of brookite, the wide peak centered around 43º corresponding to the overlapping of (022) and (221) brookite diffractions, and other less intense bands at higher 2θ degrees.

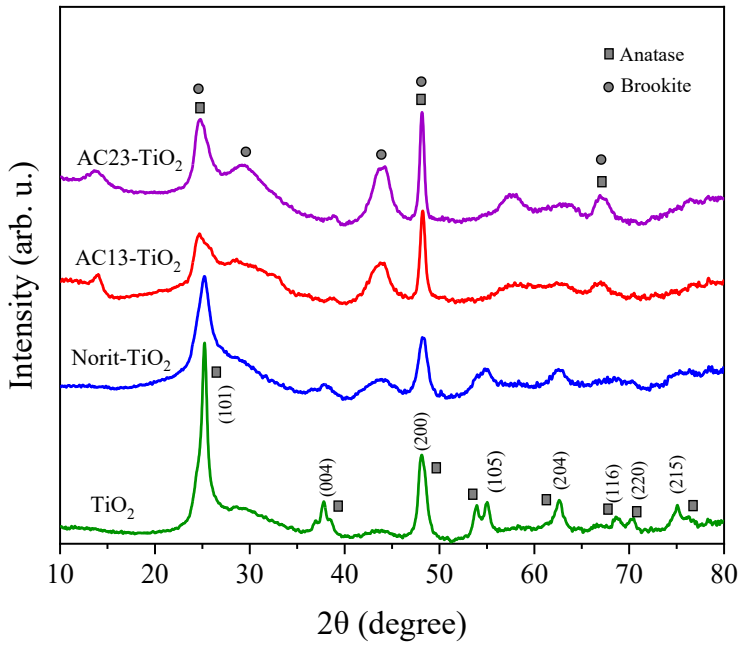

Figure 2. XRD patterns of TiO_2 NRs, Norit-TiO_2, AC13-TiO_2 and AC23-TiO_2.

The UV-Vis absorption spectra of pure TiO_2 and carbon-TiO_2 composites are depicted in Figure S4a. For all the samples, a strong band at ca. < 400 nm corresponding to the intrinsic band-gap transition of TiO_2 was observed. Moreover, it is noteworthy that all carbon-TiO_2 samples showed an enhanced absorption at wavelengths higher than 380 nm (visible range) in comparison with pure TiO_2. This effect can be associated to the electronic transitions between both phases [27]. Figure S4b exhibits the Tauc´s plots versus the energy (eV), and the calculated band gap energy (E_g) [28] for TiO_2, Norit-TiO_2, AC13-TiO_2 and AC23-TiO_2. The pure TiO_2 phase presents a band-gap energy of 3.3 eV, in agreement with the previously published results [6]. When analyze the results obtained with the composites, it is noteworthy a significant decrease of the E_g values, more specifically in the case of Norit-TiO_2, where E_g decreases to values around 3.0 eV. This behavior is also observed in both AC13-TiO_2 and AC23-TiO_2 composites, although E_g values only decrease to around 3.2 eV. These differences can be associated to the different crystalline phases present in each sample, as previously described. Comparing to anatase (3.2 eV), rutile band gap energy is well-known to be of 3.0 eV, and brookite a band gap between 3.0 and 3.6 eV [7].

3.2. Adsorption and photocatalytic performance

In Figure 3a, the behaviour of samples as ethylene adsorbents under dynamic experimental conditions is presented by the corresponding breakthrough curves. The breakthrough points of biocarbons are higher than Norit, denoting a higher adsorption capacity. It is noteworthy that, with the exception of the AC23 support, where the breakthrough curve presents a smaller slope, there is very little difference between the breakthrough and saturation points, which denote a very small concentration gradient in the front advance of the ethylene through the column. The parameters obtained from the analysis of these curves (amount of ethylene adsorbed at C/C_0= 0.90, $X_{0.90}$) are shown in Figure 3b. As expected, the adsorption capacity at breakthrough and saturation point is lower for the composites than their analogous ACs. Both AC13 and AC23, and the corresponding AC13-TiO_2 and AC23-TiO_2 composites exhibited the highest ability to adsorb ethylene compared with Norit and Norit-TiO_2 (Figure 3b).

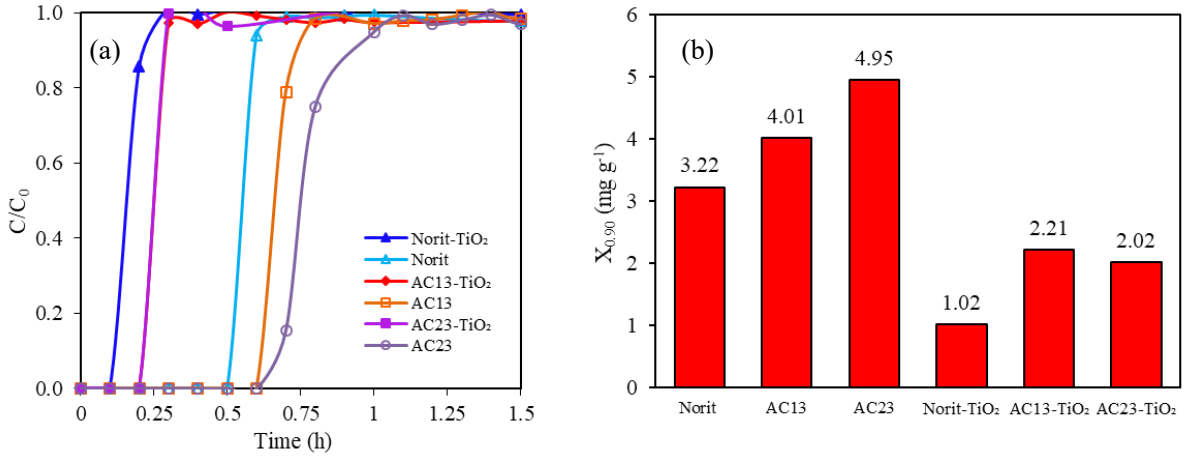

Figure 3. Breakthrough curves for ethylene adsorption (1000 vppm, 50 cm^3 min^{-1}) (a) and adsorbed amount at saturation point, C/C_0= 0.90 (b).

The ethylene adsorptive character of the ACs and composites is related with the available surface area (Figure 4a), although the performance seems to be enhanced also by increasing the acidic character of their surface. Nevertheless, the best correlations were obtained when the adsorption capacity is related only to the microporous surface (Figure 4b) obtained by applying the Stoeckli equation to both CO_2 or N_2 isotherms rather than typical S_{BET} values, which present a marked influence of large micropores and

mesopores, where N_2 can be adsorbed at – 196 ºC, but not other molecules with higher saturation pressure. These results are in agreement with those previously exposed [29, 30].

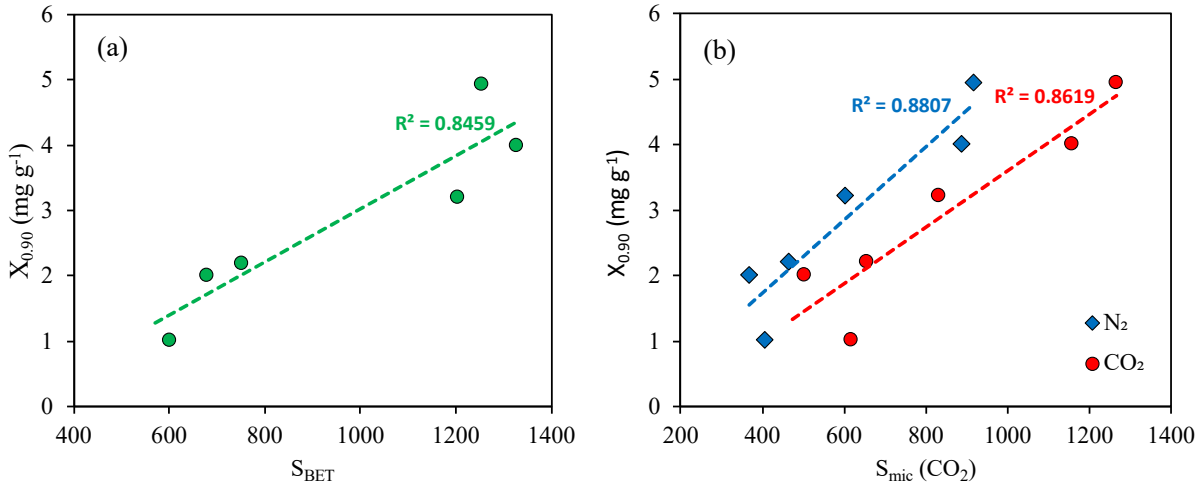

Figure 4. Variation of ethylene adsorption capacity in saturation point with BET surface area (a) and microporous surface (CO_2 and N_2) (b).

The photocatalytic oxidation of ethylene was performed at ambient temperature and continuous mode. Firstly, the reactor is feed with the gas mixture during the dark step until the photocatalyst saturation (constant C_2H_4 concentration) and then, the lamp is turned on. The experiments were performed under near UV-Vis irradiation and under UV-Vis, latter resulting in a higher photon flow entering the reactor. Firstly, only CO_2 was detected as unique gaseous reaction product (no CO_2 was detected in dark phase), thus conversion values were calculated either based on the amount of C_2H_4 removed or CO_2 formed, taking into account the reaction stoichiometry. Figure 5a depicts the good agreement between C_2H_4 conversion and CO_2 formation for the Norit-TiO_2 composite under UV-Vis irradiation, the highest differences being found for conversions determined for the CO_2 formation probably due to the fluctuations of the adsorption and desorption cycles of products.

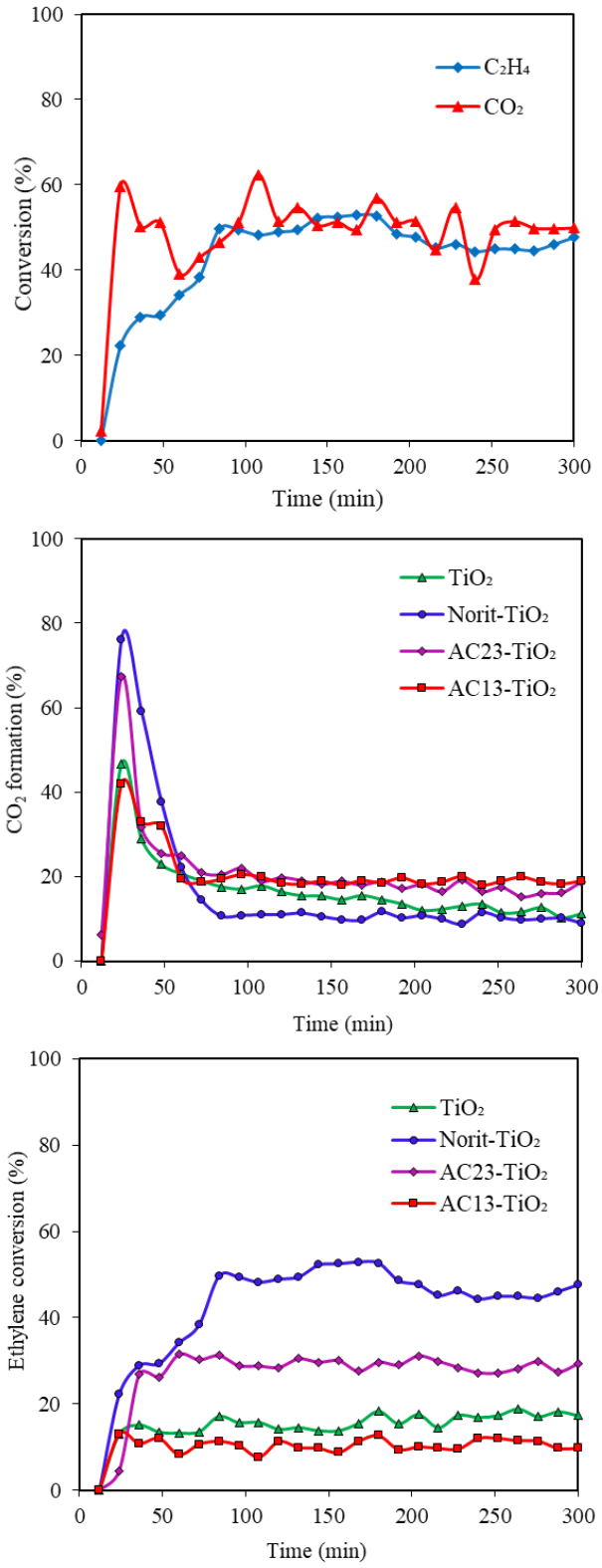

Figure 5. Photocatalytic degradation of ethylene: (a) conversions calculated from C_2H_4 removed and CO_2 formed for the Norit-TiO_2 composite under UV-Vis irradiation; (b) CO_2 conversions obtained for all photocatalysts under near UV-Vis irradiation; and (c) C_2H_4 conversion obtained under UV-Vis

irradiation. Operating conditions: feed concentration = 50 vppm; flow rate = 25 cm^3 min^{-1}, room temperature.

Results obtained under near UV-Vis and UV-Vis irradiation are shown in Figures 5b and 5c, respectively. When photooxidation reaction is performed under near UV-Vis irradiation (Figure 5b), the activity is quite similar for both biocarbon-TiO_2 composites, which were more active than Norit-TiO_2 or even, the pure TiO_2 nanorods, confirming the expected synergetic effect. At the beginning of the reaction, the amount of CO_2 formed is very high due to the oxidation of previously adsorbed C_2H_4 during the dark period. Nevertheless all the samples reached a steady state after 2 h of reaction, achieving conversion values between 15–22% for at least 5 h, which confirm the absence of photocatalyst deactivations in any case. Clearly, the oxidation efficiency increased using a quartz reactor (Figure 5c), in such a way that the total UV-Vis radiation from lamp can be used. Under these experimental conditions, the ethylene removal reached 50% in the stationary state when used Norit-TiO_2 and with exception of AC13-TiO_2, all composites improved the performance of pure TiO_2 material.

In general, it is proven that various parameters, such as crystallite size, specific surface area, pore structure, pore volume, and crystalline phases have significant effects on the photocatalytic performance [7]. The AC13-TiO_2 composite was the less crystalline sample. On the other hand, mixtures of brookite and anatase with a nanostructure composed by nanorods were detected, namely when used biocarbons as supports. It has been observed that a combination of the phases of TiO_2 has an effect on improving its activity and properties. For example, the synergistic effect between the anatase and rutile phases in P25 is attributed to the improved separation of UV-light generated photocarriers. It is generally accepted that the photoexcited electrons (e^-) in rutile migrate to the conduction band of anatase, and the photoexcited holes remain in rutile, whereas others authors observed the opposite way of electrons transference [18]. Brookite is the least studied TiO_2 phase due to the difficulties in being obtained, although it has been also reported that this phase also had a good physicochemical activity in photocatalysis [18].

The photocatalytic oxidation of ethylene applied to the storage system of perishable fruits was reviewed by Pathak et al. [31]. Most of the photocatalysts analysed were based on TiO_2, which in general report

low efficiency for ethylene removal. Doping with noble metals (Au, Ag, Pd), non-metallic heteroatoms (N, C) or use of supports (zeolites, silica and specifically carbon materials) can increase the efficiency of these materials. The reactor design (fixed bed, membranes, thin films, and so on) and the working conditions (temperature, humidity, oxygen, type of radiation, fluxes, catalyst mass, etc.) also have to be optimised. In general, it is difficult to make comparisons between the different photocatalytic systems studied, given the variability of these conditions. Some recently published catalytic systems are shown in Table 2. Many kinetic studies are carried out in batch reactors [6, 32, 33], thus avoiding the analytical problems associated with the low conversions obtained in continuous flow systems. Different semiconducting oxides [6, 33, 34] based on Zn, W, Bi and Cu are shown as alternative photocatalysts to TiO_2 as well as the use of supported or composite materials. The use of 2D carbon materials, such as graphene oxide or reduced graphene oxide (RGO) combined with TiO_2 [32, 35], shows the synergistic effect between phases, obtaining high conversions (up to 95% in flow under UV and humidity conditions). However, there are low references related with the use of biomolecules (cellulose, starch) or even biocarbons obtained from biowaste in the production of photocatalytic composites. Another aspect to be considered is the reaction products, which can vary from 100% CO_2 to a mixture of CO_2, acetaldehyde, ethanol, ethane, and C_3 and C_4 hydrocarbons also with possible effects on the conservation of the fruits [32]. In this manuscript, we show preliminary results about the development of cheap C/TiO_2 composites using bioresidues as raw materials with suitable adsorption and photocatalytic performance towards the selective ethylene removal to CO_2 under continuous flow and humidity conditions.

Table 2. Compilation of recently published works regarding different photocatalysts for ethylene removal.

Photocatalysts	Light source	Concentration/flow	Conversion	ref
ZnO /RGO (1-5% RGO)	Simulated sunlight, 300 W Xe lamp	C_2H_4 (90 µL)/ O_2 (5 mL). Static fixed bed reactor	100% to CO_2	[32]
RGO/black TiO_2	UV and visible light	25 cm^3 min^{-1}, 80 ppmv of ethylene/ 20,000 ppmv O_2/ balanced in argon	60% under Visible and 95% under UV, humidity conditions	[35]
Bi_2WO_6–TiO_2 /starch nanocomposite	Xe lamp, a UV cutoff filter (λ > 400 nm)	Static fixed bed reactor. 2 mL of high-purity C_2H_4/ 2 L cylindrical vessel	< 13%	[6]
TiO_2-Bi_2WO_6	Xe lamp (500W), UV cut-off filter (λ >400 nm)	Static fixed bed reactor	< 20.90 %	[33]
Copper oxide supported on silica	High-pressure, Hg lamp (100 W) cut off filter (λ > 280 nm)	Ethylene (0.5 kPa, 18 µmol) and water (0.5 kPa, 18 µmol). Static condition	< 1.6%. Carbon dioxide, acetaldehyde, ethanol, ethane, and C_3 and C_4 hydrocarbons are formed	[34]
Silica-supported catalysts (1 wt% and 0.5 wt% Pt 1.0 wt% Ru	Ambient lighting	C_2H_4 (50 ppm)/ static from stored fruits	Decomposition rate is constant and independent of the ethylene concentration	[36]

4. Conclusions

The removal of ethylene from air streams was studied with highly porous ACs obtained by physical activation of olive stones, which were used as ethylene adsorbents and as TiO_2 supports in the preparation of highly porous and nanostructured carbon-TiO_2 photocatalysts by hydrothermal treatments for ethylene photooxidation. A commercial AC from Norit was also used as reference and P25 (Evonik-Aeroxide) as the raw TiO_2 material.

ACs were microporous, while mesoporous TiO_2 nanorods were obtained, mainly constituted by anatase. This TiO_2 nanostructure is also obtained inside the large cavities of ACs from lignocellulosic materials (olive stones), which confers a large micro/mesoporosity to the composites, while a mixture of brookite and anatase is obtained after hydrothermal recrystallization. TiO_2 remains as spherical anatase nanoparticles using commercial ACs without development of the mesoporosity.

The removal of ethylene by adsorption is mainly governed by the narrow microporosity of the samples, increasing linearly with the microporous surface. Nevertheless, the worst correlations are obtained when use the typical BET surface area. Adsorption capacity can be also favoured by the acidity of the surfaces. All the composite materials are also active in the photooxidation of ethylene. This process is selective to CO_2 and evidently, the activity of the samples is favoured using UV-Vis radiation regarding the near-UV-Vis one. Independently of the radiation, composites are more active than the pure TiO_2 nanorods, confirming the synergetic effects between phases. These synergies can be also enhanced by the developed mesoporosity and mixture of nanostructured anatase-brookite phases obtained in the biocarbon-TiO_2 nanocomposites. Although the preparation method, reactors, illumination systems, etc. should be optimized, cheap biocarbons-TiO_2 composites demonstrated their capacities for the ethylene removal by both adsorption and photocatalysis processes

Acknowledgements

This work was financially supported by the projects: ref. PCI2020-112045 from MCIN/AEI/10.13039/501100011033 and European Union Next Generation EU/PRTR, as part of the PRIMA Programme (Nano4Fresh project). A.M.R.-M. acknowledges the National Youth Guarantee System (nº 8165) and European Social Fund (FSE) for the training contract. S.M.-T. (RYC-2019-026634-I) and L.M.P.-M. (RYC-2016-19347) are grateful to MICIN/AEI/10.13039 /501100011033 and FSE "El FSE invierte en tu futuro" for their Ramon y Cajal research contracts. "Unidad de Excelencia Química Aplicada a Biomedicina y Medioambiente" of the University of Granada (UEQ-UGR) is gratefully acknowledged for the technical assistance.

CRediT authorship contribution statement

A.M. Regadera-Macías: Investigation, Conceptualization, Formal analysis, Methodology, Writing - original draft. **S. Morales-Torres:** Conceptualization, Data curation, Resources, Writing - review & editing, Supervision. **L.M. Pastrana-Martínez:** Conceptualization, Data curation, Resources, Writing - review & editing, Supervision. **F.J. Maldonado Hódar**: Conceptualization, Resources, Project administration, Funding acquisition, Writing - review & editing, Supervision.

Declaration of Competing Interest

The authors declare that they have no known competing financial interests or personal relationships that would influence the work reported in this paper.

References

[1] R.M. Beaudry, Effect of O_2 and CO_2 partial pressure on selected phenomena affecting fruit and vegetable quality, Postharvest Biology and Technology, 15 (1999) 293-303.

[2] N. Pathak, O.J. Caleb, C. Rauh, P.V. Mahajan, Efficacy of photocatalysis and photolysis systems for the removal of ethylene under different storage conditions, Postharvest Biology and Technology, 147 (2019) 68-77.

[3] L. Cisneros, F. Gao, A. Corma, Silver nanocluster in zeolites. ADSORPTION of ETHYLENE traces for fruit preservation, Microporous and Mesoporous Materials, 283 (2019) 25-30.

[4] A. Ebrahimi, M. Zabihzadeh Khajavi, A.M. Mortazavian, H. Asilian-Mahabadi, S. Rafiee, M. Farhoodi, S. Ahmadi, Preparation of novel nano–based films impregnated by potassium permanganate as ethylene scavengers: An optimization study, Polymer Testing, 93 (2021) 106934.

[5] Q. Zhang, C. Zhu, J. Gao, L. Wang, D. Zhao, Y. Hei, Y. Li, Microfibrous structured Au/Co_3O_4/Al-fiber catalyst for the combustion of ethylene traces, Catalysis Communications, 146 (2020) 106133.

[6] H. Wang, L. Wang, S. Ye, X. Song, Construction of Bi_2WO_6–TiO_2/starch nanocomposite films for visible-light catalytic degradation of ethylene, Food Hydrocolloids, 88 (2019) 92-100.

[7] Z. Shayegan, C.-S. Lee, F. Haghighat, TiO_2 photocatalyst for removal of volatile organic compounds in gas phase – A review, Chemical Engineering Journal, 334 (2018) 2408-2439.

[8] M. Pelaez, N.T. Nolan, S.C. Pillai, M.K. Seery, P. Falaras, A.G. Kontos, P.S.M. Dunlop, J.W.J. Hamilton, J.A. Byrne, K. O'Shea, M.H. Entezari, D.D. Dionysiou, A review on the visible light active titanium dioxide photocatalysts for environmental applications, Applied Catalysis B: Environmental, 125 (2012) 331-349.

[9] L.M. Pastrana-Martínez, S. Morales-Torres, V. Likodimos, J.L. Figueiredo, J.L. Faria, P. Falaras, A.M.T. Silva, Advanced nanostructured photocatalysts based on reduced graphene oxide–TiO_2 composites for degradation of diphenhydramine pharmaceutical and methyl orange dye, Applied Catalysis B: Environmental, 123-124 (2012) 241-256.

[10] K. Maeda, M. Higashi, D. Lu, R. Abe, K. Domen, Efficient nonsacrificial water splitting through two-step photoexcitation by visible light using a modified oxynitride as a hydrogen evolution photocatalyst, J Am Chem Soc, 132 (2010) 5858-5868.

[11] G. Liu, P. Niu, C. Sun, S.C. Smith, Z. Chen, G.Q. Lu, H.M. Cheng, Unique electronic structure induced high photoreactivity of sulfur-doped graphitic C_3N_4, J Am Chem Soc, 132 (2010) 11642-11648.

[12] W. Kim, T. Tachikawa, T. Majima, W. Choi, Photocatalysis of Dye-Sensitized TiO_2 Nanoparticles with Thin Overcoat of Al_2O_3: Enhanced Activity for H_2 Production and Dechlorination of CCl_4, Journal of Physical Chemistry C, 113 (2009) 10603-10609.

[13] A.K.R. Police, S.V.P. Vattikuti, Y.-J. Baik, B. Chan, Eco-friendly, hydrogen fluoride-free, morphology-oriented synthesis of TiO_2 with exposed (001) facets, Ceramics International, 45 (2019) 2178-2184.

[14] S. Morales-Torres, L.M. Pastrana-Martínez, J.L. Figueiredo, J.L. Faria, A.M.T. Silva, Design of graphene-based TiO_2 photocatalysts-a review, Environmental Science and Pollution Research, 19 (2012) 3676-3687.

[15] L.M. Pastrana-Martínez, S. Morales-Torres, S.K. Papageorgiou, F.K. Katsaros, G.E. Romanos, J.L. Figueiredo, J.L. Faria, P. Falaras, A.M.T. Silva, Photocatalytic behaviour of nanocarbon–TiO_2 composites and immobilization into hollow fibres, Applied Catalysis B: Environmental, 142-143 (2013) 101-111.

[16] W. Wang, P. Serp, P. Kalck, C.G. Silva, J.L. Faria, Preparation and characterization of nanostructured MWCNT-TiO_2 composite materials for photocatalytic water treatment applications, Materials Research Bulletin, 43 (2008) 958-967.

[17] Y. Ao, J. Xu, D. Fu, X. Shen, C. Yuan, Low temperature preparation of anatase TiO_2-coated activated carbon, Colloids and Surfaces A: Physicochemical and Engineering Aspects, 312 (2008) 125-130.

[18] M. Hussain, N. Russo, G. Saracco, Photocatalytic abatement of VOCs by novel optimized TiO_2 nanoparticles, Chemical Engineering Journal, 166 (2011) 138-149.

[19] S. Kumar, A.G. Fedorov, J.L. Gole, Photodegradation of ethylene using visible light responsive surfaces prepared from titania nanoparticle slurries, Applied Catalysis B: Environmental, 57 (2005) 93-107.

[20] X. Dai, Y. Wang, X. Wang, S. Tong, X. Xie, Polarity on adsorption and photocatalytic performances of N-GR/TiO_2 towards gaseous acetaldehyde and ethylene, Applied Surface Science, 485 (2019) 255-265.

[21] K.-L. Chang, K. Sekiguchi, Q. Wang, F. Zhao, Removal of Ethylene and Secondary Organic Aerosols Using UV-C254 + 185 nm with TiO2 Catalyst, Aerosol and Air Quality Research, 13 (2013) 618-626.

[22] M. Hussain, S. Bensaid, F. Geobaldo, G. Saracco, N. Russo, Photocatalytic Degradation of Ethylene Emitted by Fruits with TiO2 Nanoparticles, Industrial & Engineering Chemistry Research, 50 (2011) 2536-2543.

[23] H. Sayahi, K. Aghapoor, F. Mohsenzadeh, M. Mohebi Morad, H.R. Darabi, TiO_2 nanorods integrated with titania nanoparticles: Large specific surface area 1D nanostructures for improved efficiency of dye-sensitized solar cells (DSSCs), Solar Energy, 215 (2021) 311-320.

[24] R.C. Bansal, J.B. Donnet, F. Stoeckli, Active Carbon, Marcel Dekker, New York, 1988.

[25] Y. Harima, T. Fujita, Y. Kano, I. Imae, K. Komaguchi, Y. Ooyama, J. Ohshita, Lewis-Acid Sites of TiO_2 Surface for Adsorption of Organic Dye Having Pyridyl Group as Anchoring Unit, The Journal of Physical Chemistry C, 117 (2013) 16364-16370.

[26] A. Perez-Molina, S. Morales-Torres, F.J. Maldonado-Hodar, L.M. Pastrana-Martinez, Functionalized Graphene Derivatives and TiO_2 for High Visible Light Photodegradation of Azo Dyes, Nanomaterials, 10 (2020) 1106.

[27] M. Pedrosa, L.M. Pastrana-Martínez, M.F.R. Pereira, J.L. Faria, J.L. Figueiredo, A.M.T. Silva, N/S-doped graphene derivatives and TiO_2 for catalytic ozonation and photocatalysis of water pollutants, Chemical Engineering Journal, 348 (2018) 888-897.

[28] S. Morales-Torres, L.M. Pastrana-Martínez, J.L. Figueiredo, J.L. Faria, A.M.T. Silva, Graphene oxide-P25 photocatalysts for degradation of diphenhydramine pharmaceutical and methyl orange dye, Applied Surface Science, 275 (2013) 361-368.

[29] W. Liang, Y. Zhang, X. Wang, Y. Wu, X. Zhou, J. Xiao, Y. Li, H. Wang, Z. Li, Asphalt-derived high surface area activated porous carbons for the effective adsorption separation of ethane and ethylene, Chemical Engineering Science, 162 (2017) 192-202.

[30] N. Miyajima, K. Hirooka, H. Sakane, M. Furuya, K. Tamura, Y. Matsumoto, Pore structures and ethylene adsorption behavior of polysaccharide-derived carbons, Carbon, 50 (2011) 737-738.

[31] N. Pathak, O.J. Caleb, M. Geyer, W.B. Herppich, C. Rauh, P.V. Mahajan, Photocatalytic and Photochemical Oxidation of Ethylene: Potential for Storage of Fresh Produce—a Review, Food and Bioprocess Technology, 10 (2017) 982-1001.

[32] M. Huang, J. Lin, R. Li, Y. Su, X. Zhao, Y. Liu, W.-J. Chen, X. Lian, X. Chen, X. Pan, Hierarchical ZnO Nanosheet-Reduced Graphene Oxide Composites for Photocatalytic Ethylene Oxidation, ACS Applied Nano Materials, 5 (2022) 1828-1835.

[33] R. Wang, M. Xu, J. Xie, S. Ye, X. Song, A spherical TiO2-Bi2WO6 composite photocatalyst for visible-light photocatalytic degradation of ethylene, Colloids and Surfaces A: Physicochemical and Engineering Aspects, 602 (2020) 125048.

[34] Y. Ichihashi, Y. Matsumura, Partial Photooxidation of Ethylene with Water as Oxidant over Copper Oxide Supported on Silica, Journal of Catalysis, 202 (2001) 427-429.

[35] N. Pugazhenthiran, H. Valdés, R.V. Mangalaraja, P. Sathishkumar, S. Murugesan, Graphene modified “black {001}TiO2” nanosheets for photocatalytic oxidation of ethylene: The implications of chemical surface characteristics in the reaction mechanism, Separation and Purification Technology, 292 (2022) 121008.

[36] T. Mori, T. Shigyo, T. Nomura, Y. Osanai, K. Nakajima, A. Fukuoka, Ethylene oxidation activity of silica-supported platinum catalysts for the preservation of perishables, Catalysis Science & Technology, 12 (2022) 3116-3122.